CrossMark

RESEARCH PAPER

Carrageenan-grafted magnetite nanoparticles as recyclable sorbents for dye removal

**Ana L. Daniel-da-Silva · Ana M. Salgueiro · Bianca Creaney ·
Rui Oliveira-Silva · Nuno J. O. Silva · Tito Trindade**

Abstract The efforts dedicated to improving water decontamination procedures have prompted the interest in the development of efficient, inexpensive, and reusable sorbents for the uptake of dye pollutants. In this work, novel sorbents consisting of carrageenan polysaccharides grafted to magnetic iron oxide nanoparticles were prepared. κ- and ι-carrageenan were first chemically modified by carboxymethylation and then covalently attached via amide bond to the surface of aminated silica-coated magnetite nanoparticles, both steps monitored using infrared spectroscopy (FTIR) analysis. The kinetics and the equilibrium behavior of the cationic dye methylene blue (MB) adsorption onto the carrageenan sorbents were investigated. ι-carrageenan sorbents displayed higher MB adsorption capacity that was ascribed to high content of sulfonate groups. Overall, the pseudo-second order equation provided a good description of the adsorption kinetics. The κ-carrageenan sorbents followed an unusual Z-type equilibrium adsorption isotherm whereas the isotherm of ι-carrageenan sorbents, although displaying a conventional shape, could not be successfully predicted by isotherm models commonly used. Noteworthy, both sorbents were long-term stable and could easily be recycled by simply rinsing with KCl aqueous solution. The removal efficiency of κ-carrageenan sorbents was 92 % in the first adsorption cycle and kept high (>80 %) even after six consecutive adsorption/desorption cycles.

Keywords Magnetite nanoparticles ·
Polysaccharide · Carrageenan · Dye removal ·
Methylene blue · Adsorption · Environmental and
health effects

A. L. Daniel-da-Silva (✉) · A. M. Salgueiro ·
B. Creaney · R. Oliveira-Silva · T. Trindade
Department of Chemistry, CICECO, Aveiro Institute of
Materials, University of Aveiro, 3810-193 Aveiro,
Portugal
e-mail: ana.luisa@ua.pt

A. M. Salgueiro
e-mail: a38242@ua.pt

B. Creaney
e-mail: bianca.creaney@gmail.com

R. Oliveira-Silva
e-mail: ruipedro.silva@ua.pt

T. Trindade
e-mail: tito@ua.pt

N. J. O. Silva
Department of Physics, CICECO, Aveiro Institute of
Materials, University of Aveiro, 3810-193 Aveiro,
Portugal
e-mail: nunojoao@ua.pt

Introduction

Many distinct methods have been proposed for the treatment of wastewaters and the removal of organic pollutants, namely membrane processes, chemical precipitation, photochemical degradation, oxidation, and adsorption. Further details regarding the advantages and drawbacks of each method can be found elsewhere (Forgacs et al. 2004; Nguyen and Juang 2013; Nidheesh et al. 2013; Savage and Diallo 2005). Adsorption, compared with other methods appears to be a very attractive process in view of its simplicity, low cost, and efficiency. Due to economic and environmental factors, the concept of recoverable and reusable sorbents has gained importance and subsequently, the use of magnetic sorbents, namely magnetic nanoparticles (MNPs) has raised increasing interest.

MNPs are very interesting sorbents owing to their small size, low diffusion resistance, high specific area, low cost, and magnetic features that enable fast magnetic separation from solution (Xu et al. 2012; Ambashta and Sillanpaa 2010; Daniel-da-Silva et al. 2013a). Furthermore, enhanced adsorption and selectivity of the MNPs toward target pollutants can be achieved by chemical modification of the MNPs' surface with specific chemical groups that will interact with the pollutant compounds (Sousa et al. 2015; Tavares et al. 2013). Example of this approach is the surface modification of the particles with polysaccharides that contain in their structure chemical functionalities with affinity for the pollutants, such as chitosan and derivatives (Ngah et al. 2011) and alginate (Rocher et al. 2008). However the weak immobilization of the polymers onto the particles' surface can lead to poor sorbents' recyclability with loss of adsorption capacity due to polymer leaching. For example, magnetite nanoparticles coated with κ-carrageenan, a sulfonated polysaccharide (Fig. 1), was found to be an efficient material for removing the organic pollutant methylene blue (MB) from water using magnetic separation (Salgueiro et al. 2013). The efficiency was ascribed primarily to the electrostatic interaction between the sulfonate groups of carrageenan and MB, a cationic dye (Soedjak 1994). Although effective in MB removal, the polymer shell of these sorbents lacked stability and impaired reusability. This limitation should be overcome resorting to covalent bonding.
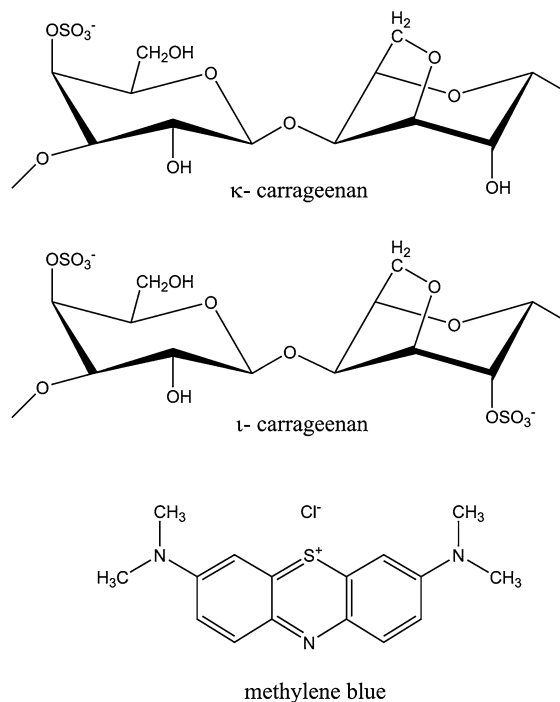

Fig. 1 Chemical structure of methylene blue dye and disaccharide repeated unit of κ-carrageenan and ι-carrageenan

This work reports the preparation of carrageenan functionalized magnetic sorbents using a distinct strategy based on the covalent immobilization of the polysaccharide onto the surfaces' particle. Carrageenan comprises a family of linear water-soluble sulfonated polysaccharides extracted from red seaweeds. Due to their biocompatibility and ability to form hydrogels, carrageenan has been extensively used as a gelling agent in food and pharmaceutical industries (Campo et al. 2009) and more recently as dye adsorbents (Salgueiro et al. 2013). In this work, carrageenan was first chemically modified for the introduction of carboxylic acid groups and then covalently attached to amino-functionalized magnetic nanoparticles. The resulting materials were then tested for the uptake of methylene blue, as a model pollutant. Methylene blue (MB) (Fig. 1), a cationic dye, is one of the most commonly used compounds for dying cotton, silk, and wood (Rafatullah et al. 2010) and hence is found in industrial wastewaters and in water streams. Although MB is less hazardous than other dyes, it has various harmful effects and acute exposure causes nausea, vomiting, abdominal discomfort, and chest pain (Oz et al. 2011). Moreover the presence of MB in

water supplies might reduce light penetration and photosynthesis that may result in death of the aquatic life. The as-prepared sorbents exhibit enhanced regeneration and reusability in MB uptake without loss of adsorption capacity. Besides κ-carrageenan, which bears one sulfonate group per disaccharide unit, the sorbents were also prepared using ι-carrageenan with high degree of sulfonation (Fig. 1).

Materials and methods

Materials

All chemicals used in this work were of analytical reagent grade and were obtained from commercial chemical suppliers and used without further purification. The polysaccharides κ-carrageenan (cat. no. 22048) and ι-carrageenan (cat. no. 22045) were purchased from Fluka Chemie (USA). Potassium chloride (KCl, >99 %), iron (III) chloride hexahydrated (FeCl$_3$.6H$_2$O, >99 %), iron (II) chloride tetrahydrate (FeCl$_2$.4H$_2$O, >99 %), trisodium citrate dihydrate (HOC(COONa)(CH$_2$COONa)$_2$·2H$_2$O, 99 %), tetraethyl orthosilicate (Si(OC$_2$H$_5$)$_4$, TEOS, >99 %), 3-aminopropyltriethoxysilane (H$_2$N(CH$_2$)$_3$Si(OC$_2$H$_5$)$_3$, APTES, >99 %), triethylamine (99 %), monochloroacetic acid (ClCH$_2$COOH, >99 %), *N*-ethyl-*N*′-(3-dimethylaminopropyl)carbodiimide hydrochloride (EDC, commercial grade), and *N*-hydroxysuccinimide (NHS, 98 %) were purchased from Sigma-Aldrich. Ammonia (NH$_4$OH) (25 % NH$_3$) and methylene blue (C$_{16}$H$_{18}$ClN$_3$S) were obtained from Riedel-de Häen. Ethanol absolute was bought from Carlo Erba and nitric acid (HNO$_3$ 25 %) was purchased from Panreac.

Preparation of the sorbents

Carboxymethylation of carrageenan

Carrageenan (1.5 g) was stirred into a mixture of isopropanol (42.5 mL), water (7.5 mL), and NaOH (4.3 g, 107.5 mmol). The mixture was left stirring at 60 °C for 1 h under reflux and N$_2$ atmosphere. Afterwards, monochloroacetic acid (3 g, 31.7 mmol) was added and the suspension was stirred for 2 h in the same conditions. After cooling to RT, solvents were removed by decanting. The solid was dissolved in warm water and then precipitated by adding

isopropanol and collected by solvent decantation. This cycle was repeated four times for purification of the modified carrageenan. Finally, the solid was filtrated under vacuum and freeze-dried. The same experimental procedure was used for the carboxymethylation of κ- and ι-carrageenan.

Preparation of amino-functionalized nanoparticles

Magnetite nanoparticles (MNPs) were prepared following the co-precipitation method, as previously reported (Ferreira et al. 2011; Salgueiro et al. 2013). Typically, 4.43 g (16.4 mmol) FeCl$_3$.6H$_2$O and 1.63 g (8.2 mmol) of FeCl$_2$·4H$_2$O were dissolved in 190 mL of distilled water at room temperature, under nitrogen atmosphere, and mechanical stirring. Afterwards 10 mL of ammonia was added to the solution and stirred for 10 min. The final solution displayed a black coloration which, together with the observed magnetic properties, indicates the presence of magnetite (Fe$_3$O$_4$). The nanoparticles were magnetically separated, and washed with distilled water.

Prior to silica encapsulation, the nanoparticles were stabilized with citrate ions. The MNPs were washed twice with an aqueous solution of HNO$_3$ 2 M, magnetically separated, washed with distilled water, and the pH was set around 2.5. Then, sodium citrate (5 mL, 0.5 M) was added to the suspension of MNPs (200 mL) and the solution was left stirring for 1 h at room temperature. Afterwards the particles were magnetically recovered, washed thoroughly with distilled water, and freeze-dried.

Silica coating of the nanoparticles was performed by hydrolysis of tetraethyl orthosilicate (TEOS) in alkaline conditions using triethylamine as catalyst. Typically, a suspension of nanoparticles (100 mg) in 18 mL of distilled water was sonicated for 10 min in a ice bath, to prevent particle aggregation followed by the addition of 1 mL (4.47 mmol) of TEOS (30 % v/v in ethanol) and 0.1 mL (0.72 mmol) de triethylamine. (Bumb et al. 2008; Ferreira et al. 2011) The reaction was performed under sonication for 15 min at room temperature and the particles were magnetically recovered as a black powder and washed thoroughly with distilled water and freeze-dried.

The coated nanoparticles (30 mg) were washed with 1-propanol and then dispersed in 3 mL of water followed by the addition of 0.1 mL (0.43 mmol) of

3-aminopropyltrimethoxysilane (APTES) (Ferreira et al. 2011; Lin et al. 2007). The mixture was incubated at room temperature for 12 h and the resulting black precipitate was magnetically recovered and washed thoroughly with distilled water and freeze-dried.

Grafting of carrageenan to MNPs

The grafting of carrageenan to functionalized MNPs was carried out following a procedure adapted from literature (Lopez-Cruz et al. 2009). Briefly, 100 mg of carboxymethyl carrageenan was added to 20 mg (0.10 mmol) of EDC and 25 mg (0.22 mmol) of NHS and stirred until a homogenous solution was achieved, for activation of the carboxyl groups. Then, amino-functionalized nanoparticles (70 mg) dispersed in 5 ml of water were added. The pH was set in the range 4–5, and the resulting suspension was stirred for 24 h, at room temperature. The nanoparticles were magnetically separated, rinsed with distilled water, and freeze-dried.

Characterization of the materials

The crystalline phase of the MNPs was identified by X-ray diffraction (XRD). The X-ray powder diffraction patterns of the lyophilized samples were recorded using a X-ray diffractometer Philips X'Pert equipped with a $CuK\alpha$ monochromatic radiation source.

Fourier transform infrared (FTIR) spectra of the carrageenan and functionalized nanoparticles were collected using a spectrometer Bruker optics tensor 27 coupled to a horizontal attenuated total reflectance (ATR) cell, using 256 scans at a resolution of 4 cm^{-1}. Elemental analysis for carbon, nitrogen, hydrogen, and sulfur was performed using a LECO CHNS-932 elemental analyzer. The morphology and size of the NPs were investigated by transmission electron microscopy (TEM) using a transmission electron microscope Hitachi 9000 operating at an accelerating voltage of 300 kV. Samples for TEM analysis were prepared by evaporating dilute suspensions of the nanoparticles on a copper grid coated with an amorphous carbon film. The specific surface area of the nanoparticles was determined with nitrogen adsorption BET measurements performed with a Gemini Micromeritics instrument. Hydrodynamic particle size was measured by Dynamic Light Scattering (DLS) and zeta potential was measured by electrophoretic light scattering, both using a Zetasizer Nanoseries instrument from Malvern Instruments. DLS and zeta potential measurements were performed in stable suspensions diluted with ultrapure water at 25 °C. Magnetization of the lyophilized samples of bare Fe_3O_4, $Fe_3O_4@SiO_2$, and carrageenan-grafted nanoparticles was recorded as a function of the applied magnetic field at 300 K. All measurements were performed on a MPMS 5 s (Quantum Design) magnetometer equipped with a reciprocal sample measurement system.

Adsorption experiments

The ability of functionalized MNPs to uptake methylene blue (MB) from water was evaluated by batch adsorption experiments. The general procedure was performed as follows. Accurately weighted amounts of functionalized MNPs were added to a MB aqueous solution of known concentration prepared with deionized water and shaken using a FALC F205 rotator at 36 rpm under isothermal conditions (23 ± 1 °C). This time was considered the starting point of the experiment. Aliquots were collected for analysis at known times, and the NPs were separated using a NdFeB magnet. The MB concentration in the supernatant was determined using UV–Vis spectroscopy by recording samples absorbance at 663 nm, in a Hitachi U-2000 UV–Vis spectrophotometer. Prior to UV–Vis analysis, the aliquots were diluted with KCl 1 M to ensure that all MB present in the solution was in the free form (Daniel-da-Silva et al. 2012).

The amount of MB adsorbed into the coated NPs at time t (q_t, mg/g) was derived from the mass balance between the initial MB concentration and the concentration at time t in solution, as displayed by Eq. (1), where C_0 (mg/L) is the initial concentration of MB, C_t is the concentration of MB at time t, V is the total volume (L), and m is the mass of the dried coated NPs (g).

$$q_t = (C_0 - C_t) \times \frac{V}{m} \tag{1}$$

Control experiments performed without NPs were also carried out to confirm that the MB adsorption on glass material was negligible.

The effect of pH on MB removal

In order to determine the optimal pH solution for MB adsorption, the MB removal was evaluated at variable pH, in the range 2–11. Generally, the pH of MB solution (20 mL, 20 mg/L) was adjusted to the required value by adding HCl or NH₄OH. Then, 10 mg of the coated MNPs was added and dispersed, and the batch experiment was run in the conditions described above. The final concentration of MB was determined by UV–Vis spectroscopy. The pH of the solution was also measured at the end the adsorption experiment to confirm that no pH of significant variations arise from the addition of the MNPs.

Kinetic experiments

The time profile of MB adsorption onto MNPs was assessed in order to investigate the kinetics of adsorption. Typically, 20 mg of functionalized MNPs (accurately weighted) was added to the MB solution (40 mL, 20 mg/L) with pH previously adjusted to 10. The mixture was shaken, and aliquots were collected along the time, at 20 °C. The amount of MB adsorbed onto the MNPs at each time interval (q_t, mg/g) was determined and plotted against time (t, min) for kinetic modeling.

Equilibrium isotherms experiments

Equilibrium isotherms were obtained by dispersing ca. 2.5 mg (accurately weighted) of coated MNPs in 5 ml solution with variable initial MB concentration (2, 5,10, 25, 40, 50, 70, 80, 100, 120, 150, and 200 mg/L) pH 10. The experiments were conducted at 20 °C for 2 h and performed in triplicate. The amount of MB adsorbed at equilibrium (q_e, mg/g) was assessed by UV–Vis spectroscopy and calculated using Eq. 1 for $C = C_e$.

Desorption and reuse after desorption

The MB-loaded nanoparticles used in the adsorption experiments were collected and rinsed with KCl (1 M, 5 mL) and separated magnetically. The process was repeated until no MB absorption was detected in the visible adsorption spectrum of the supernatant, typically for 5 times. Then, the nanoparticles were rinsed with distilled water and magnetically separated.

To investigate the reusability of the adsorbents, the nanoparticles after desorption were reused in adsorption experiments. The process was repeated four times and the removal percentage was calculated after a contact time of 2 h.

Kinetics modeling

Kinetics studies provide valuable insights about the adsorption rates and mechanisms. The kinetic adsorption data were fitted to three kinetic equations commonly used in the study of adsorption processes, the pseudo-first order equation (Lagergren 1898), the pseudo-second order equation (Ho and McKay 1999), and the Elovich model (Roginsky and Zeldovich 1934). These models are given by Eqs. (2), (3), and (4) respectively, where k_1 (min⁻¹) is the pseudo-first order rate constant and k_2 (g/mg/min) is the of pseudo-second order rate constant. The parameters a (mg/g/min) and b (g/mg) are constants of the Elovich model, the former related to the initial adsorption rate.

$$q_t = q_e\left(1 - e^{-k_1 t}\right) \tag{2}$$

$$q_t = \frac{k_2 q_e^2 t}{1 + k_2 q_e t} \tag{3}$$

$$q_t = \frac{1}{b}\ln(1 + abt) \tag{4}$$

The pseudo-first order equation has been widely used to predict the adsorption of solutes from liquid solutions in systems near equilibrium and in systems with a time-independent solute concentration or linear behavior in equilibrium adsorption isotherms (Soto et al. 2011). The pseudo-second-order kinetic equation, in contrast with the previous model, usually predicts the behavior over the whole range of adsorption (Ho and McKay 1999). The Elovich model (Roginsky and Zeldovich 1934) neglects the rate of simultaneously occurring desorption and it is suitable for describing the adsorption kinetics in heterogeneous adsorbing surfaces and in systems with mildly rising tendency (Plazinski et al. 2009).

Equilibrium isotherm modeling

Equilibrium isotherm models allow estimating the adsorption capacity of the adsorbent and provide valuable information about the interaction between

the adsorbate and the adsorbent at the equilibrium, at fixed temperature. The equilibrium data were fitted to three frequently used isotherm models, the Langmuir, the Freundlich, and the Sips isotherm model.

The Langmuir isotherm was initially proposed to describe gas–solid adsorption onto activated carbon (Langmuir 1918). Nowadays it is commonly used to describe the adsorption in different bio-sorbents (Foo and Hameed 2010) assuming monolayer adsorption on a homogeneous surface (Langmuir 1918; Foo and Hameed 2010). The non-linear form of this model is given by Eq. (5)

$$q_e = \frac{q_m k_L C_e}{1 + K_L C_e}, \tag{5}$$

where q_e (mg/g) is the amount of solute adsorbed at equilibrium, C_e (mg/L) is the concentration of the solute at equilibrium, q_m (mg/g) is the monolayer adsorption capacity per unit of adsorbent, and k_L (L/mg) is the Langmuir adsorption constant.

Another frequently applied isotherm model is the Freundlich isotherm that assumes multilayer adsorption, with non-uniform distribution of adsorption heat and affinities over the heterogeneous surface (Foo and Hameed 2010; Freundlich 1906). Usually, it is applied in describing heterogeneous systems such as the adsorption of organic compounds or highly interactive species on activated carbon and molecular sieves (Foo and Hameed 2010). The non-linear form of the Freundlich model is given by Eq. (6)

$$q_e = k_F C_e^{1/n}, \tag{6}$$

where k_F ($mg^{(1-1/n)}$ $L^{(1/n)}$ g^{-1}) is the Freundlich constant and $1/n$ is the heterogeneity factor which varies between 0 and 1.

The Sips isotherm model combines the characteristics of Langmuir and Freundlich isotherms (Sips 1948). It was deducted for predicting the heterogeneous adsorption systems. At high solute concentrations, this model predicts the monolayer adsorption capacity as in the Langmuir model, whereas at low solute concentrations it reduces to Freundlich model. The non-linear form of the Sips model is given by Eq. (7)

$$q_e = \frac{k_S C_e^{\beta_S}}{1 + a_S C_e^{\beta_S}}, \tag{7}$$

where K_s (L/g) and a_s (L/mg) are the Sips isotherm model constants and α_S is the Sips isotherm model exponent.

Error analysis

Experimental data were fitted with the non-linear form of kinetic and isotherm equations, using the method of least squares and the tool *solver* of the *excel* software. The goodness of the fitting was evaluated based on the analysis of the correlation coefficient (R^2), expressed by the Eq. (8)

$$R^2 = 1 - \frac{\sum_{i=1}^{n}(y_i - \hat{y}_i)^2}{\sum_{i=1}^{n}(y_i - \bar{y})^2}, \tag{8}$$

where y_i and $\hat{y}_i$ are the experimental and model predicted values, respectively, $\bar{y}$ is the mean of the experimental data, and n is the sample size.

Results and discussion

Characterization of the sorbents

The structure of carrageenan polysaccharides was modified by carboxymethylation following a procedure previously implemented for κ-carrageenan (Daniel-da-Silva et al. 2009). The ATR-FTIR spectra of the carrageenan polysaccharides, before and after carboxymethylation (Fig. 2), show a typical
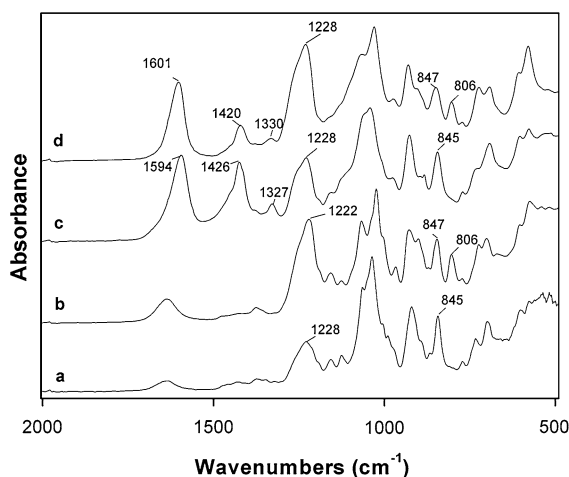

Fig. 2 ATR-FTIR spectra of κ- and ι-carrageenan before (**a, b,** respectively) and after carboxymethylation (**c, d,** respectively)

carrageenan absorption band around 1225 cm^{-1} corresponding to the S–O asymmetric stretch.

Furthermore, broad absorption bands, due to C–O and C–OH vibrations characteristic of polysaccharides, are observed in the 1040–1070 cm^{-1} region. κ- and ι-carrageenan show a clear band at around 845 cm^{-1} corresponding to the α(1-3)-D-galactose C–O–S stretch. ι-carrageenan has an additional band around 806 cm^{-1} due to the sulfate group in the 3,6-anhydrogalactose-2-sulfate unit (Prado-Fernandez et al. 2003; Pereira et al. 2003). New vibrational bands appear in the spectra of modified carrageenan at ca. 1420 and 1600 cm^{-1} that were assigned to the symmetric and asymmetric stretching vibration of carboxylate (–COO$^-$) groups (Daniel-da-Silva et al. 2009; Tranquilan-Aranilla et al. 2012; Coleman et al. 1990), respectively, and confirm the introduction of carboxymethyl groups in the structure of carrageenan. Moreover a new band appears at ca. 1325 cm^{-1} that was assigned to the –CH$_2$ scissoring in the carboxymethyl group (Tranquilan-Aranilla et al. 2012).

The magnetic core of the MNPs consisted in magnetic iron oxide nanoparticles that were obtained by co-precipitation of Fe(II) and Fe(III) in alkaline conditions, a method that has been reported to yield magnetite. (Cornell and Schwertmann 2006) Indeed, the powder X-ray diffractogram of the black precipitate obtained (Fig. S1—Supplementary Material) matched the typical diffraction patterns observed for magnetite (Fe$_3$O$_4$). The average size of the magnetite nanoparticles was estimated from the XRD results using a modified version of Scherrer's equation (Borchert et al. 2005; Daniel-da-Silva et al. 2007) and was found to be 9.8 nm. The nanoparticles were then coated with amorphous silica to prevent particle clustering and to ensure their chemical stability. Prior to silica encapsulation, the nanoparticles were stabilized with citrate ions (Bumb et al. 2008; Ferreira et al. 2011). Silica coating of the nanoparticles was performed by hydrolysis of tetraethyl orthosilicate (TEOS) in alkaline conditions using triethylamine as catalyst. TEM analysis of the silica-coated nanoparticles (Fe$_3$O$_4$@SiO$_2$) shows magnetite nanoparticles with an average size of 11.8 ± 3.2 nm (the inner dark core), in agreement with Scherrer's equation size estimation, and the presence of a silica shell around the magnetic core with few nanometers (<5 nm) in thickness (Fig. 3-inset).

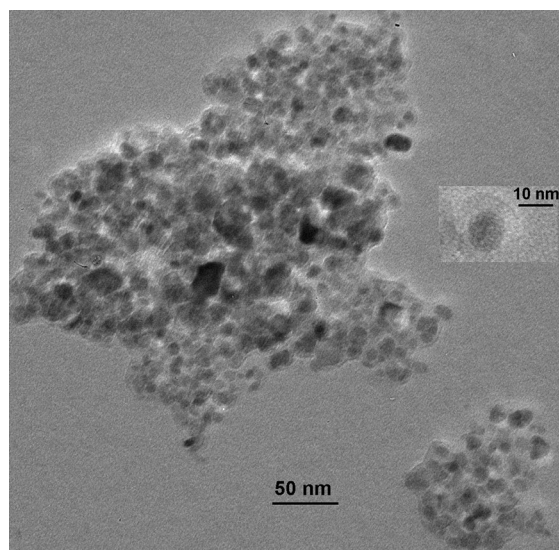**Fig. 3** TEM image of Fe$_3$O$_4$@SiO$_2$ nanoparticles

Subsequently, the surface of the Fe$_3$O$_4$@SiO$_2$ nanoparticles was functionalized with amine groups via hydrolysis and condensation of 3-aminopropyltriethoxysilane (APTES). Then, the carboxymethyl carrageenan was covalently attached to the surface of the amino-functionalized nanoparticles (MNPs-NH$_2$) via a carbodiimide-mediated reaction using *N*-ethyl-*N*′-(3-dimethylaminopropyl)carbodiimide hydrochloride (EDC) and *N*-hydroxysuccinimide (NHS). Hereafter, the magnetic particles functionalized with carboxymethyl κ- and ι-carrageenan will be designated by MNPs-kappa and MNPs-iota, respectively. A scheme of the whole magnetite surface modification is shown in the Fig. 4.

Successful synthesis and surface modification of the nanoparticles was monitored step-by-step by ATR-FTIR spectroscopy (Fig. 5). The ATR-FTIR spectrum of citrate stabilized Fe$_3$O$_4$ nanoparticles shows typical vibrational bands assigned to the stretching of Fe–O at 530 cm^{-1} (Cornell and Schwertmann 2006) and to the asymmetric stretching of –COO$^-$ at 1555 cm^{-1} and the stretching of –CO groups at 1340 cm^{-1} (Fig. 5a) (Coleman et al. 1990). Although less intense, the bands of citrate at 1600 and 1390 cm^{-1} also appear in the spectra of samples obtained in the subsequent steps but showing slight shifts, thus indicating that citrate is still present in residual amounts. The silica coating was confirmed by the appearance of a band at 1053 cm^{-1} assigned to Si–O-Si asymmetric stretching
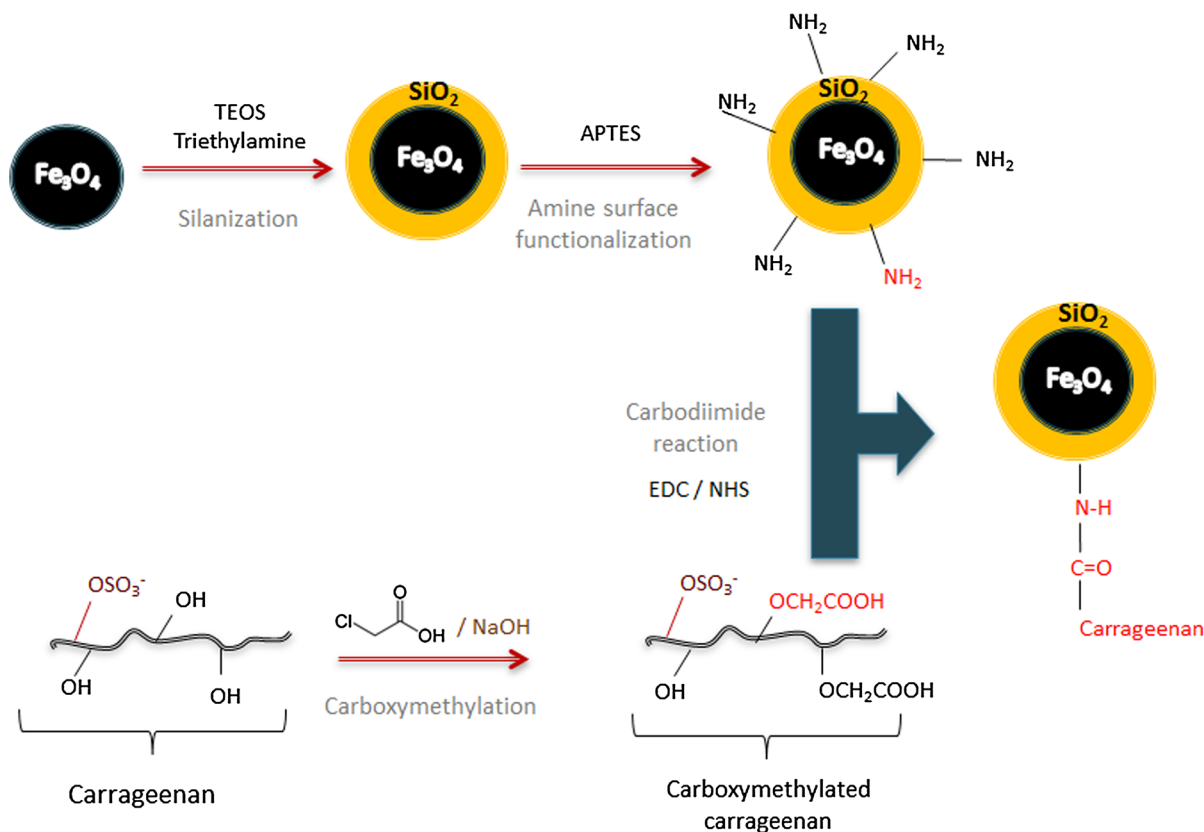
Fig. 4 Scheme of the chemical strategy used for the modification of the surface of Fe$_3$O$_4$ nanoparticles

(Fig. 5a) (Daniel-da-Silva et al. 2008b; Girginova et al. 2010). Amine surface functionalization was verified by the observation of a band at 1560 cm^{-1} ascribed to N–H bending vibration (De Palma et al. 2007), by the appearance of a shoulder at 1130 cm^{-1} assigned to C-N stretching modes (Bruce and Sen 2005) and a broad band centered at 2875 cm^{-1} assigned to the stretching of C-H bonds of the propyl group in APTES (De Palma et al. 2007) (Fig. 5a).

The spectra of the nanoparticles after the reaction with carboxymethyl carrageenan (Fig. 5b) show the characteristic vibrational bands of the polymer at 1230 cm^{-1} (S–O asymmetric stretch) thus confirming the presence of these polysaccharides at the surface of the nanoparticles. A new band appears in the amide II region at 1538 cm^{-1} due to the N–H bending mode vibration coupled to stretching C-N vibrations (Bruce and Sen 2005; Daniel-da-Silva et al. 2013b). Also a weak band appears at 1260 cm^{-1} in the amide III region, also assigned to the C–N stretching and N–H bending (Pelton and McLean 2000). These results are

consistent with the covalent attachment of the carrageenan to the surface of the nanoparticles, via an amide bond. The bands at 1713 and 1414 cm^{-1} were assigned to the stretching vibration of the H-bonded C=O groups (Daniel-da-Silva et al. 2008a; Tranquilan-Aranilla et al. 2012) and to symmetric stretching vibration of carboxylate groups (Coleman et al. 1990; Daniel-da-Silva et al. 2009; Tranquilan-Aranilla et al. 2012), respectively. The appearance of these bands suggests the presence in the final materials of –COOH groups that did not react during the carbodiimide reaction.

Elemental microanalysis results, specific surface area, and the zeta potential of the nanoparticles are shown in Table 1 and Table S1 (supplementary material). As expected, the nanoparticles modified with carrageenan contain sulfur that arises from the polysaccharide. The zeta potential of the amine-functionalized MNPs decreases after the attachment of the carrageenan due to the anionic nature of these polysaccharides (Table 1). Moreover, the zeta
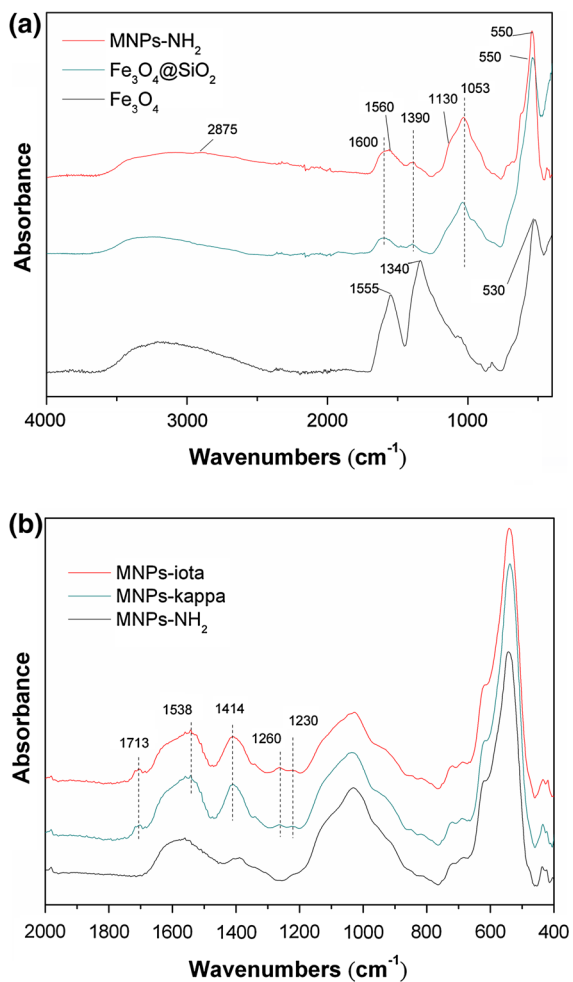
Fig. 5 ATR-FTIR spectra of **a** citrate-stabilized magnetite, silica-coated magnetite, and amine surface-functionalized silica-coated nanoparticles and **b** magnetic nanoparticles functionalized with amine groups and covalently linked to carboxymethylated carrageenans

carrageenans. The presence of carboxylic acid groups, as denoted by FTIR analysis, will also contribute to the negative surface charge of the particles. The increase of BET specific surface area is also in agreement with surface modification with polysaccharide chains.

The magnetic properties of bare magnetite (Fe_3O_4) and surface-modified particles were assessed by SQUID magnetometer measurements. At $T = 300$ K, the nanoparticles of all samples exhibited superparamagnetic unblocked behavior, with no hysteresis loop (i.e., zero remanence and coercive field, Fig. 6).

The magnetization saturation was 70.0 emu/g_{sample} for bare Fe_3O_4 nanoparticles which is close to the values reported in the literature for spherical magnetite nanoparticles with similar size (Goya et al. 2003), and slightly decreased to 64 emu/g_{sample} after silica coating, as expected due to the increase of the diamagnetic fraction of the sample. Overall the grafting of carrageenans to the surface of the nanoparticles did not affect significantly their susceptibility and saturation magnetization, as illustrated in Fig. 6 for the case of MNPs-kappa sample.

Dye removal experiments

Carrageenan-functionalized magnetic nanoparticles were fabricated following a rational design that aims their application as sorbents for the uptake of the cationic dye methylene blue from waters. The magnetic core of Fe_3O_4 confers magnetic characteristics to the resulting sorbents that makes them suitable and relevant for simple magnetically assisted separation of pollutants from water. Encapsulation within amorphous SiO_2 shells prevents the oxidation of the magnetic core, eventually increasing the robustness of the sorbent. Finally, carrageenan molecules attached to the surface of nanoparticles are expected to provide affinity for MB molecules, due to

potential absolute values and the ratio S/N follow the tendency kappa < iota which is in agreement with the increasing number of sulfate/disaccharide units in

Table 1 Elemental microanalysis, BET surface area (S_{BET}), and zeta potential (ζ) of modified magnetic nanoparticles

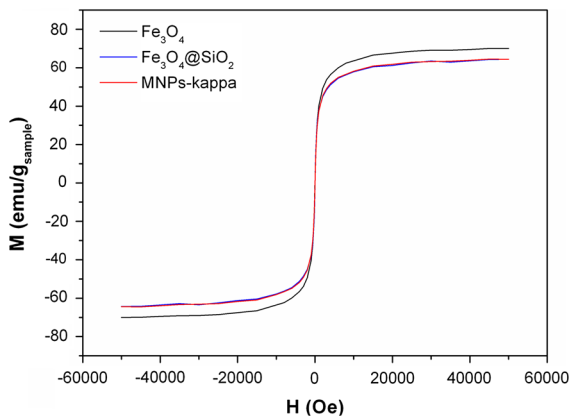| Samples	N (%)	S (%)	S/N	S_{BET} (m^2/g)	ζ (mV)
MNPs-NH$_2$	0.43	–	–	71.4 ± 1.7	−12.3 ± 2.1 (pH 6.5)
MNPs-kappa	0.26	0.08	0.31	170.0 ± 2.9	−14.2 ± 1.2 (pH 6.0)
MNPs-iota	0.37	0.40	1.08	170.6 ± 3.1	−21.1 ± 1.4 (pH 6.2)

Fig. 6 Magnetization of the nanoparticles as a function of the magnetic field applied, at 300 K

electrostatic interactions between the anionic sulfonate groups of carrageenan and cationic MB molecules (Soedjak 1994). Carrageenan was covalently attached to the surface of the nanoparticles aiming to achieve recyclability without loss of adsorption capacity due to carrageenan leaching. In addition, dimensions of the resulting materials were kept at nanoscale in order to confer high specific surface area which when combined with carrageenan functionalization should provide enhanced MB adsorption capacity. Thus, the carrageenan functionalized magnetic nanoparticles characterized as in the above section were investigated for MB uptake from water.

The effect of pH on MB removal

Figure 7a displays the effect of the pH solution on the MB removal ability of the carrageenan functionalized MNPs. The removal percentage was calculated using Eq. (9)

$$\text{Removal } (\%) = \frac{(C_0 - C_e)}{C_0} \times 100, \qquad (9)$$

where C_e (mg/L) is the concentration of MB at equilibrium time.

The MB removal percentage of the MNPs functionalized with carrageenan increases by increasing the pH and, as expected, MB uptake is higher at alkaline pH than in acidic conditions. This behavior was previously observed for MB removal by magnetic nanoparticles coated with κ-carrageenan (Salgueiro

et al. 2013) and was attributed to the deprotonation of $-SO_3^-$ groups with pH increase, that will interact electrostatically with MB, as well as to the existence of less protons at high pH that could otherwise compete with MB for the negatively charged groups of carrageenan. Identical pH effect has also been observed for MB removal using sorbents modified with anionic surfactants containing $-SO_3^-$ groups (Aksu et al. 2010; Jin et al. 2008). This also agrees with the observation that at alkaline pH the MNPs-iota removed more MB than MNPs-kappa, thus consistent with the higher sulfonate content of the MNPs functionalized with ι-carrageenan. As such, the kinetic studies and adsorption isotherms for the MNPs functionalized with carrageenans were conducted at pH 10 because high removal percentages were observed in these conditions.

The effect of the contact time and kinetic studies

Figure 7b shows the time profile of the MB uptake by the NPs for variable initial MB concentration of 10 and 100 mg/L, at 23 °C. The MNPs functionalized with carrageenan show ability to uptake MB from the solution, while the adsorption of MB on the MNPs functionalized with amine groups (NPs prior to the functionalization with polysaccharide) is negligible thus confirming that the MB adsorption takes place at carrageenan. The MB adsorption can be ascribed to the electrostatic interaction between the sulfonate groups of carrageenan and the methylene blue molecules (Soedjak 1994). The adsorption equilibrium is reached within approximately 90 min. Differences on the adsorption capacity at equilibrium (q_e) are more evident for an initial MB concentration of 100 mg/L, the MNPs-iota showing higher q_e than MNPs-kappa.

The adsorption kinetics was investigated and the experimental data were fitted with three well-known kinetic models, the pseudo-1st order and pseudo-2nd order kinetic equations and the Elovich model, given by Eqs. (2), (3), and (4) respectively. The kinetic parameters and the evaluation of the goodness of the fits are reported in Table 2. Based on the correlation coefficients (R^2), the experimental data fit better the Elovich model (MNPs-iota $C_0 = 10$ mg/L) and the pseudo-2nd order equation (for the remaining conditions tested). The best kinetic fitting are shown in Fig. 7b.

Fig. 7 **a** Influence of the pH solution on the amount of MB removed by the sorbents (C_{0MB} = 5 mg/L). **b** Effect of contact time on adsorption (C_{0MB} = 10 and 100 mg/L) and best kinetic fitting. Isotherm of the adsorption of MB onto **c** MNPs-kappa and **d** MNPs-iota
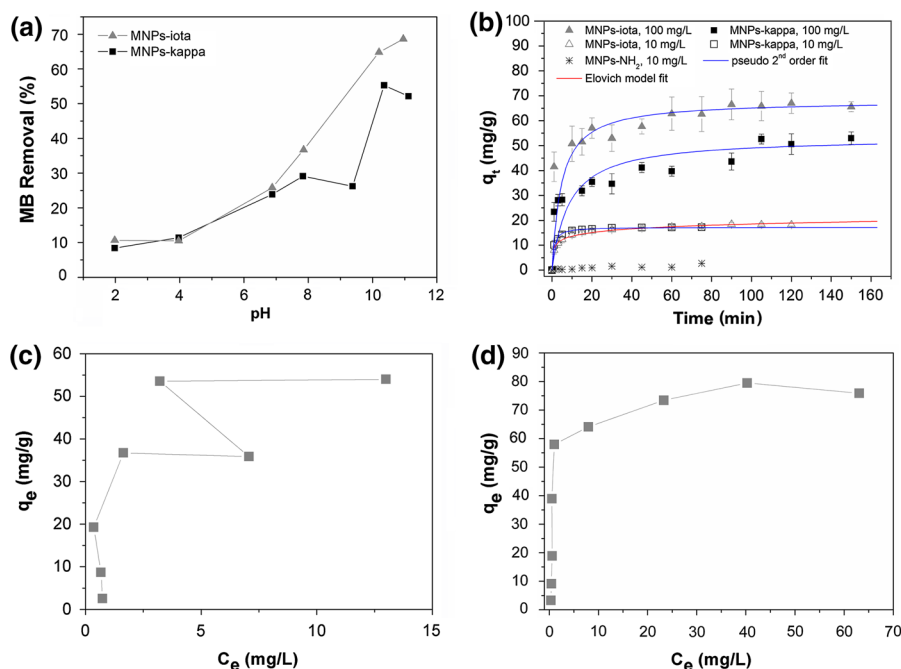

Table 2 Kinetic parameters estimated from pseudo 1st and 2nd order equations and Elovich model and evaluation of its fittings for an initial MB concentration of 10 and 100 mg/L

C_0 (mg/L)	Sample	q_e exp (mg/g)	Model parameters								
			Pseudo-1st order equation			Pseudo-2nd order equation			Elovich model		
			q_e (mg/g)	k_1 (min^{-1})	R^2	q_e (mg/g)	k_2 (g/mg/min)	R^2	a (mg/g min)	b (g/mg)	R^2
10	MNPs-kappa	17.2	16.45	0.687	0.9584	17.27	0.067	0.9933	1407.02	0.6087	0.9819
	MNPs-iota	19.1	17.13	0.325	0.9144	18.20	0.027	0.9670	132.96	0.4726	0.9918
100	MNPs-kappa	53.0	41.92	0.3778	0.7654	53.19	0.0022	0.9806	205.88	0.1749	0.9341
	MNPs-iota	65.6	60.04	1.1757	0.89826	68.03	0.0032	0.9975	7216.14	0.1836	0.9852

Adsorption equilibrium isotherms

The isotherm experimental data for MB adsorption onto MNPs functionalized with κ- and ι-carrageenan are shown in Fig. 7. The isotherm of MNPs-kappa displays a Z-type shape (Fig. 7c). For this sorbent, there is an initial MB concentration threshold (C_0 = 25 mg/L) above which the equilibrium concentration (C_e) decreases with increasing C_0 values, and thus the isotherm curve reverses. Such C_e decrease indicates that the MB uptake increases suddenly most probably because more sulfonate groups from carrageenan became available to interact with MB molecules. Indeed, in our recent work devoted to the

study of the removal of MB using magnetic nanoparticles with κ-carrageenan molecules adsorbed onto the surface we have also reported this unusual type of adsorption isotherm (Salgueiro et al. 2013). This behavior was attributed to the formation of MB aggregates in MB concentrated solutions, which can cause the disruption of the carrageenan network by electrostatic interaction with the sulfonated polyelectrolytes, thus exposing to the solution sulfonate groups that were not available before (Moreno-Villoslada et al. 2009; Salgueiro et al. 2013).

The isotherm of the sorbent MNPs-iota displays a different shape (Fig. 7d). The experimental data were fitted to the Langmuir, Freundlich, and Sips equations

that are described by the Eqs. 4, 5, and 6, respectively. The model parameters estimated are listed in Table 3.

Among these three models, the Sips isotherm is the most suitable because the correlation coefficient (R^2) was much higher. However, even for the Sips model the obtained R^2 value was still low (0.933) meaning that this model fails in predicting the isotherm behavior. In an attempt to find a model that better describes the equilibrium adsorption, the data were fitted using other two-parameter and three-parameter models of isotherm adsorption: Hill, Dubinin–Radushkevich, Redlich–Peterson, Khan, Radke–Prausnitz, and Toth isotherm models. Further details about these models can be found elsewhere (Foo and Hameed 2010; Liu and Liu 2008). The R^2 value was always low (<0.900) thus indicating that all these models failed in describing the isotherm data of the sorbent MNPs-iota.

Desorption and reuse

Although recycling and reuse of the sorbents is of great importance in certain practical applications, these features are sometimes neglected when evaluating the performance of highly efficient sorbents. Here, this aspect was particularly appraised by exploring a chemical surface modification strategy that could result in robust sorbents for regeneration purposes. Thus, desorption experiments were firstly conducted to evaluate if the MNPs could be regenerated and then reused as sorbents. Because carrageenans and MB form complexes that are less stable in high ionic strength medium (Soedjak 1994) an aqueous solution of the electrolyte KCl (1 M) was used for the regeneration of the MNPs. Desorption of MB from MB-loaded MNPs was monitored by UV–Vis analysis of the KCl solution (data not shown). Then, the MNPs underwent consecutive adsorption–desorption experiment cycles. The adsorption experiments were carried out at initial MB concentrations that yield high MB recovery efficiency in the isotherm studies for each adsorbent sample, thus being 20 and 30 and 100 mg/L for MNPs functionalized with κ- and ι-carrageenan, respectively. The MB removal of the MNPs after 6 cycles is shown in Fig. 8.

The MB removal ability of MNPs-kappa slightly decreased from 91.8 to 88.3 % after the first desorption step, and kept high (83.4 %) even after six consecutive adsorption/desorption cycles. Therefore, the sorbent MNPs-kappa could effectively remove methylene blue from aqueous solution with high efficiency and shows reusability. MNPs-iota also shows reusability on the removal of MB whereas the regeneration capacity seems to be lower when compared to the particles functionalized with κ-carrageenan. Indeed the MB removal ability of MNPs-iota decreased gradually from 96.6 to 67.1 % after six cycles, which can be attributed to the incomplete MB desorption from the surface of MNPs-iota. This can be ascribed to the higher reactivity between MB and ι-carrageenan (Soedjak 1994). Overall, the results show that the covalent attachment of the carrageenan to the surface of the MNP is a successful strategy to impart reusability to the sorbents for MB removal.

Comparison with other sorbents

The maximum MB adsorption capacity (q_{max}) of the carrageenan-grafted magnetic nanoparticles was 54 mg/g (MNPs-kappa) and 77 mg/g (MNPs-iota), at 23 °C and pH 10. For comparison, Table 4 lists the MB adsorption capacity of other magnetic sorbents reported in literature.

Note that some of the biopolymer-based magnetic sorbents displayed higher MB q_{max} than those reported in this work but the reusability of the sorbents was not assessed. The maximum adsorption capacity of the sorbents developed in this work is lower than q_{max} of

Table 3 Parameters calculated from the Langmuir, Freundlich, and Sips isotherm models for the adsorption of MB onto MNPs-iota

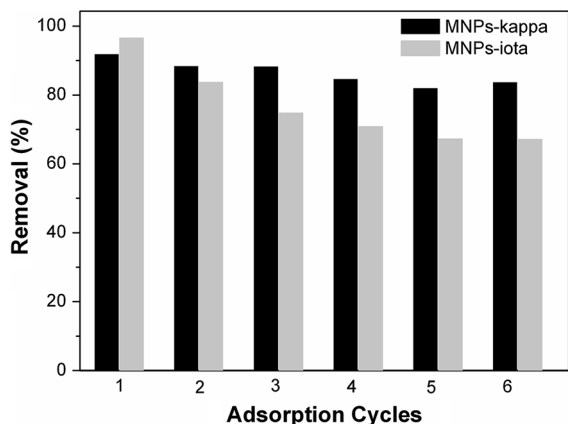| Langmuir		Freundlich		Sips	
q_{max} (mg/g)	77.77	K_F ((mg/g)(mg/L)^n)	32.49	a_s (L/mg)	4.254
K_L (L/g)	0.929	n	4.28	β_s	3.487
R^2	0.8268	R^2	0.7039	K_s (L/g)	308.3
				R^2	0.9330

Fig. 8 Removal of MB after consecutive adsorption/desorption cycles

κ-carrageenan-coated magnetite nanoparticles, also reported by our group (Salgueiro et al. 2013). This can be explained by the lower amount of carrageenan molecules attached to the surface of the NPs using the covalent immobilization strategy reported here, when compared to the simple carrageenan coating used in our previous work. However, it should be noted that the covalent grafting of the polysaccharide onto the MNPs provides the advantage of reusability of such

magnetic sorbents without significant loss of adsorption capacity after several adsorption cycles.

Unlike other magnetic sorbents that show comparable q_{max} values for MB, carrageenan-functionalized sorbents reported here are recyclable upon rinsing with KCl aqueous solutions, instead of using NaOH, HCl, and organic solvents (Shi et al. 2013; Zhang et al. 2014).

Conclusions

κ- and ι-carrageenan-grafted magnetic nanoparticles were successfully prepared and investigated as magnetic nano-sorbents for the uptake of MB from water. Among the sorbents tested, MNPs-iota exhibited greater adsorption capacity (77 mg/g) due to high content of sulfonate groups that can interact electrostatically with MB molecules. Both sorbent materials provided fast MB removal (<2 h), easy separation from solution through the application of an external magnetic field, and simple regeneration using KCl solutions. Owing to the covalent immobilization of the carrageenan to the magnetic support, the particles MNPs-kappa were reusable for six adsorption cycles without significant loss of the adsorption capacity. In

Table 4 Maximum MB adsorption capacities (q_{max}) of several magnetic sorbents reported in literature, including the carrageenan-derivatized particles investigated here

Adsorbent	Efficient reusability	Regeneration medium	pH	T (°C)	q_{max} (mg/g)	Reference
MNPs-kappa	Yes	KCl (aq)	10	23	54	This work
MNPs-iota	Yes	KCl (aq)	10	23	77	This work
κ-Carrageenan-coated MNPs	No	KCl (aq)	9	23	185.3	Salgueiro et al. (2013)
Fe$_3$O$_4$/Cellulose/GO	Yes	NaOH (aq)	6	25	70.0	Shi et al. (2013)
Fe$_3$O$_4$ hollow silica spheres	Yes	HCl/Ethanol (pH 2)	7	25	71.5	Zhang et al. (2014)
Magnetic alginate beads crosslinked with EP	Not tested	–	7.5	n.a.	223.9	Rocher et al. (2010)
CMCD–MNP(P)	Not tested	–	12	25	277.8	Badruddoza et al. (2010)
CMCD–MNP(C)					140.8	
Fe$_3$O$_4$-loaded MWCNTs	Not tested	–	n.a.	25	48.1	Ai et al. (2011)
Fe$_3$O$_4$ NPs coated with PGA	Not tested	–	6	28	78.7	Inbaraj and Chen (2011)
SiO$_2$@NiO core–shell NPs	Not tested	–	n.a.	RT	53.0	Bayal and Jeevanandam (2013)

GO Graphene oxide; *EP* epichlorohydrin; *CMCD–MNP(P), CMCD–MNP(C)* carboxymethyl-β-cyclodextrin linked to Fe$_3$O$_4$ NPs prepared by one-step and two-step method, respectively; *MWCNTs* multiwall carbon nanotubes; *PGA* poly(γ-glutamic acid)

principle, this chemical surface strategy can be implemented using other polysaccharide coatings envisaging reusable sorbents without the loss of adsorption capacity.

References

Ai LH, Zhang CY, Liao F, Wang Y, Li M, Meng LY, Jiang J (2011) Removal of methylene blue from aqueous solution with magnetite loaded multi-wall carbon nanotube: kinetic, isotherm and mechanism analysis. J Hazard Mater 198:282–290

Aksu Z, Ertuğrul S, Dönmez G (2010) Methylene blue biosorption by Rhizopus arrhizus: effect of SDS (sodium dodecylsulfate) surfactant on biosorption properties. Chem Eng J 158:474–481

Ambashta RD, Sillanpaa M (2010) Water purification using magnetic assistance: a review. J Hazard Mater 180:38–49

Badruddoza AZM, Hazel GSS, Hidajat K, Uddin MS (2010) Synthesis of carboxymethyl-beta-cyclodextrin conjugated magnetic nano-adsorbent for removal of methylene blue. Colloid Surf A-Physicochem Eng Asp 367:85–95

Bayal N, Jeevanandam P (2013) Synthesis of SiO$_2$@NiO magnetic core–shell nanoparticles and their use as adsorbents for the removal of methylene blue. J Nanopart Res 15(2066):1–15

Borchert H, Shevchenko EV, Robert A, Mekis I, Kornowski A, Grübel G, Weller H (2005) Determination of nanocrystal sizes: a comparison of TEM, SAXS, and XRD studies of highly monodisperse CoPt$_3$ particles. Langmuir 21:1931–1936

Bruce IJ, Sen T (2005) Surface modification of magnetic nanoparticles with alkoxysilanes and their application in magnetic bioseparations. Langmuir 21:7029–7035

Bumb A, Brechbiel MW, Choyke PL, Fugger PL, Eggeman A, Prabhakaran D, Hutchinson J, Dobson PJ (2008) Synthesis and characterization of ultra-small superparamagnetic iron oxide nanoparticles thinly coated with silica. Nanotechnology 19:1–6

Campo VL, Kawano DF, da Silva DB, Carvalho I (2009) Carrageenans: biological properties, chemical modifications and structural analysis—a review. Carbohyd Polym 77:167–180

Coleman MM, Lee JY, Painter PC (1990) Acid salts and the structure of ionomers. Macromolecules 23:2339–2345

Cornell RM, Schwertmann U (2006) The iron oxides: structure, properties, reactions, occurrences and uses, 2nd edn. Wiley-VCH, Weinheim

Daniel-da-Silva AL, Trindade T, Goodfellow BJ, Costa BFO, Correia RN, Gil AM (2007) In situ synthesis of magnetite nanoparticles in carrageenan gels. Biomacromolecules 8:2350–2357

Daniel-da-Silva AL, Bordado JCM, Martín-Martínez JM (2008a) Moisture curing kinetics of isocyanate ended urethane quasi-prepolymers monitored by IR spectroscopy and DSC. J Appl Polym Sci 107:700–709

Daniel-da-Silva AL, Pinto F, Lopes-da-Silva JA, Trindade T, Goodfellow BJ, Gil AM (2008b) Rheological behavior of thermoreversible κ-carrageenan/nanosilica gels. J Colloid Interf Sci 320:575–581

Daniel-da-Silva AL, Fateixa S, Guiomar AJ, Costa BFO, Silva NJO, Trindade T, Goodfellow BJ, Gil AM (2009) Bio-functionalized magnetic hydrogel nanospheres of magnetite and κ-carrageenan. Nanotechnology 20, article number 355602, 1–10

Daniel-da-Silva AL, Moreira J, Neto R, Estrada AC, Gil AM, Trindade T (2012) Impact of magnetic nanofillers in the swelling and release properties of kappa-carrageenan hydrogel nanocomposites. Carbohyd Polym 87:328–335

Daniel-da-Silva AL, Carvalho RS, Trindade T (2013a) Magnetic hydrogel nanocomposites and composite nanoparticles—a review of recent patented works. Recent Pat Nanotech 7:153–166

Daniel-da-Silva AL, Salgueiro AM, Trindade T (2013b) Effects of Au nanoparticles on thermoresponsive genipin-cross-linked gelatin hydrogels. Gold Bull 46:25–33

De Palma R, Peeters S, Van Bael MJ, Van den Rul H, Bonroy K, Laureyn W, Mullens J, Borghs G, Maes G (2007) Silane ligand exchange to make hydrophobic superparamagnetic nanoparticles water-dispersible. Chem Mater 19:1821–1831

Ferreira JA, Daniel-da-Silva AL, Alves RMP, Duarte D, Vieira I, Santos LL, Vitorino R, Amado F (2011) Synthesis and optimization of lectin functionalized nanoprobes for the selective recovery of glycoproteins from human body fluids. Anal Chem 83:7035–7043

Foo KY, Hameed BH (2010) Insights into the modeling of adsorption isotherm systems. Chem Eng J 156:2–10

Forgacs E, Cserháti T, Oros G (2004) Removal of synthetic dyes from wastewaters: a review. Environ Int 30:953–971

Freundlich H (1906) Concerning adsorption in solutions. Zeitschrift Fur Physikalische Chemie-Stochiometrie Und Verwandtschaftslehre 57:385–470

Girginova PI, Daniel-da-Silva AL, Lopes CB, Figueira P, Otero M, Amaral VS, Pereira VS, Trindade T (2010) Silica coated magnetite particles for magnetic removal of Hg^{2+} from water. J Colloid Interf Sci 345:234–240

Goya GF, Berquo TS, Fonseca FC, Morales MP (2003) Static and dynamic magnetic properties of spherical magnetite nanoparticles. J Appl Phys 94:3520–3528

Ho YS, McKay G (1999) Pseudo-second order model for sorption processes. Process Biochem 34:451–465

Inbaraj BS, Chen BH (2011) Dye adsorption characteristics of magnetite nanoparticles coated with a biopolymer poly(-gamma-glutamic acid). Bioresource Tech 102:8868–8876

Jin X, Jiang M-Q, Shan X-Q, Pei Z-G, Chen Z (2008) Adsorption of methylene blue and orange II onto unmodified and surfactant-modified zeolite. J Colloid Interf Sci 328:243–247

Lagergren SY (1898) *Zur Theorie der sogenannten Adsorption gelöster Stoffe*

Langmuir I (1918) The adsorption of gases on plane surfaces of glass, mica and platinum. J Am Chem Soc 40:1361–1403

Lin PC, Tseng MC, Su AK, Chen YJ, Lin CC (2007) Functionalized magnetic nanoparticles for small-molecule isolation, identification, and quantification. Anal Chem 79:3401–3408

Liu Y, Liu Y-J (2008) Biosorption isotherms, kinetics and thermodynamics. Sep Purif Technol 61:229–242

Lopez-Cruz A, Barrera C, Calero-DdelC VL, Rinaldi C (2009) Water dispersible iron oxide nanoparticles coated with covalently linked chitosan. J Mater Chem 19:6870–6876

Moreno-Villoslada I, Torres C, González F, Shibue T, Nishide H (2009) Binding of methylene blue to polyelectrolytes containing sulfonate groups. Macromol Chem Phys 210:1167–1175

Ngah WSW, Teong LC, Hanafiah M (2011) Adsorption of dyes and heavy metal ions by chitosan composites: a review. Carbohyd Polym 83:1446–1456

Nguyen TA, Juang R-S (2013) Treatment of waters and wastewaters containing sulfur dyes: a review. Chem Eng J 219:109–117

Nidheesh P, Gandhimathi R, Ramesh S (2013) Degradation of dyes from aqueous solution by Fenton processes: a review. Environ Sci Pollut Res 20:2099–2132

Oz M, Lorke DE, Hasan M, Petroianu GA (2011) Cellular and molecular actions of methylene blue in the nervous system. Med Res Rev 31:93–117

Pelton JT, McLean LR (2000) Spectroscopic methods for analysis of protein secondary structure. Anal Biochem 277:167–176

Pereira L, Sousa A, Coelho H, Amado AM, Ribeiro-Claro PJA (2003) Use of FTIR, FT-Raman and ^{13}C-NMR spectroscopy for identification of some seaweed phycocolloids. Biomol Eng 20:223–228

Plazinski W, Rudzinski W, Plazinska A (2009) Theoretical models of sorption kinetics including a surface reaction mechanism: a review. Adv Colloid Interfac 152:2–13

Prado-Fernandez J, Rodriguez-Vazquez JA, Tojo E, Andrade JM (2003) Quantitation of kappa-, iota- and lambda-carrageenans by mid-infrared spectroscopy and PLS regression. Anal Chim Acta 480:23–37

Rafatullah M, Sulaiman O, Hashim R, Ahmad A (2010) Adsorption of methylene blue on low-cost adsorbents: a review. J Hazard Mater 177:70–80

Rocher V, Siaugue J-M, Cabuil V, Bee A (2008) Removal of organic dyes by magnetic alginate beads. Water Res 42:1290–1298

Rocher V, Bee A, Siaugue JM, Cabuil V (2010) Dye removal from aqueous solution by magnetic alginate beads crosslinked with epichlorohydrin. J Hazard Mater 178:434–439

Roginsky S, Zeldovich Y (1934) Acta Phys Chim USSR 1:554

Salgueiro AM, Daniel-da-Silva AL, Girão AV, Pinheiro PC, Trindade T (2013) Unusual dye adsorption behavior of κ-carrageenan coated superparamagnetic nanoparticles. Chem Eng J 229:276–284

Savage N, Diallo MS (2005) Nanomaterials and water purification: opportunities and challenges. J Nanopart Res 7:331–342

Shi H, Li W, Zhong L, Xu C (2013) Methylene blue adsorption from aqueous solution by magnetic cellulose/graphene oxide composite: equilibrium, kinetics, and thermodynamics. Ind Eng Chem Res 53:1108–1118

Sips R (1948) On the structure of a catalyst surface. J Chem Phys 16:490–495

Soedjak HS (1994) Colorimetric determination of carrageenans and other anionic hydrocolloids with methylene-blue. Anal Chem 66:4514–4518

Soto ML, Moure A, Domínguez H, Parajó JC (2011) Recovery, concentration and purification of phenolic compounds by adsorption: a review. J Food Eng 105:1–27

Sousa FL, Daniel-da-Silva AL, Silva NJO, Trindade T (2015) Bionanocomposites for the magnetic removal of water pollutants. In: Thakur vK, Thakur MK (eds) Eco-friendly polymer nanocomposites: chemistry and applications. Springer, Cambridge

Tavares DS, Daniel-da-Silva AL, Lopes CB, Silva NJO, Amaral VS, Rocha J, Pereira E, Trindade T (2013) Efficient sorbents based on magnetite coated with siliceous hybrid shells for removal of mercury ions. J Mater Chem A 1:8134–8143

Tranquilan-Aranilla C, Nagasawa N, Bayquen A, Dela Rosa A (2012) Synthesis and characterization of carboxymethyl derivatives of kappa-carrageenan. Carbohyd Polym 87:1810–1816

Xu PA, Zeng GM, Huang DL, Feng CL, Hu S, Zhao MH, Lai C, Wei Z, Huang C, Xie GX, Liu ZF (2012) Use of iron oxide nanomaterials in wastewater treatment: a review. Sci Total Environ 424:1–10

Zhang J, Li B, Yang W, Liu J (2014) Synthesis of magnetic Fe$_3$O$_4$@hierarchical hollow silica nanospheres for efficient removal of methylene blue from aqueous solutions. Ind Eng Chem Res 53:10629–10636